Severe Liver Degeneration in Mice Lacking the IκB Kinase 2 Gene

Qiutang Li,[1] Daniel Van Antwerp,[1] Frank Mercurio,[2] Kuo-Fen Lee,[1] Inder M. Verma[1]*

Phosphorylation of inhibitor of kappa B (IκB) proteins is an important step in the activation of the transcription nuclear factor kappa B (NF-κB) and requires two IκB kinases, IKK1 (IKKα) and IKK2 (IKKβ). Mice that are devoid of the IKK2 gene had extensive liver damage from apoptosis and died as embryos, but these mice could be rescued by the inactivation of the gene encoding tumor necrosis factor receptor 1. Mouse embryonic fibroblast cells that were isolated from IKK2$^{-/-}$ embryos showed a marked reduction in tumor necrosis factor–α (TNF-α)– and interleukin-1α–induced NF-κB activity and an enhanced apoptosis in response to TNF-α. IKK1 associated with NF-κB essential modulator (IKKγ/IKKAP1), another component of the IKK complex. These results show that IKK2 is essential for mouse development and cannot be substituted with IKK1.

The transcription factor NF-κB orchestrates expression of a large number of genes that are essential for growth, differentiation, and development (*1*). When cells are stimulated by TNF-α and interleukin-1 (IL-1), IκB proteins associated with NF-κB in the cytoplasm become phosphorylated, ubiquitinated, and degraded. Degradation of IκB proteins frees NF-κB proteins, which then translocate into the nucleus, where they activate transcription (*2*). IκB proteins (IκBα and IκBβ) are phosphorylated by a 700- to 900-kD IκB kinase (IKK) complex (*3–5*). Two kinases in this complex, IKK1 and IKK2, phosphorylate IκBα at Ser^{32} and Ser^{36} (*3, 4, 6, 7*). To investigate the requirement of IKK2 in NF-κB activation during development, we inactivated IKK2 in mice by targeted gene disruption.

The gene encoding IKK2 was inactivated by replacing two exons that encode amino acids 36 through 106 with a DNA fragment containing phosphoglycerokinase-neomycin (PGK-neo) (Fig. 1A). Southern (DNA) blot (Fig. 1B) and polymerase chain reaction (PCR) analyses (Fig. 1C) were used to identify targeted embryonic stem (ES) clones and to genotype IKK2 mutant mice, respectively (*8*). Two ES clones were germ line–transmitted. Heterozygous IKK2 mutant mice appeared normal, viable, and fertile. However, no homozygous IKK2 mutant mice were identified among 87 pups from heterozygous intercrosses. The ratio of wild-type (+/+): heterozygous (+/–):homozygous (–/–) mutant mice was 31:56:0 (1:1.9:0), indicating that IKK2$^{-/-}$ mice were embryonically lethal. Examination of embryos at various times during gestation revealed that IKK2$^{-/-}$ embryos died between embryonic day 12.5 (E12.5)

[1]Salk Institute, La Jolla, CA 92037, USA. [2]Signal Pharmaceuticals, San Diego, CA 92121, USA.

*To whom correspondence should be addressed. E-mail: verma@salk.edu

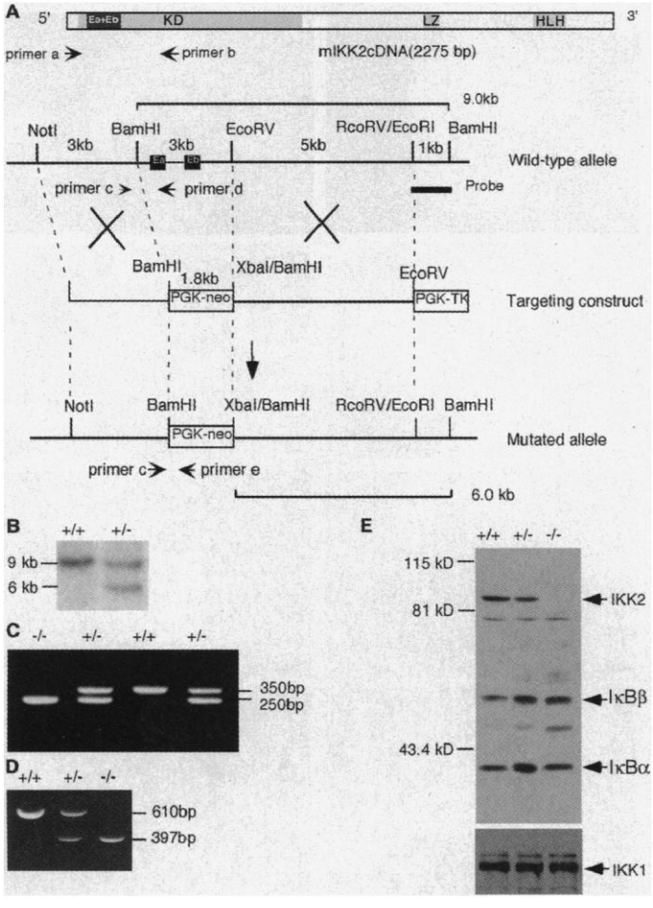

Fig. 1. Generation of IKK2$^{-/-}$ null mice (*8*). (**A**) The targeting vector was designed to replace the two exons (Ea and Eb) that encode part of IKK2 kinase domain (KD), including the ATP-binding site at Lys^{44}. In the targeting construct, the 3-kb Bam HI to Eco RV genomic fragment was replaced by a 1.8-kb PGK-neo cassette. LZ, leucine zipper region; HLH, helix-loop-helix region. (**B**) Southern blot analysis of Bam HI–digested DNA with a probe [indicated in (A)] revealed the expected 9-kb fragment from the wild-type locus and the 6-kb fragment from the targeted locus. (**C**) PCR-based genotyping of E13 embryos from heterozygous mating. Primers c, d, and e are shown in (A) and described in (*8*). Genomic DNAs were isolated from yolk sacs. (**D**) RT-PCR analysis of total RNA from untreated MEF cells of IKK2 wild-type (+/+), heterozygous (+/–), and homozygous (–/–) embryos with primers a and b [shown in (A)]. Primer a is 5′-ATGTCCTCAGCGGGTGTCG, and the reverse primer b is 5′-CAACGGTCACGGTGTACTTC. RT-PCR products were cloned into pCR II-TOPO vector (Invitrogen) and subjected to automated DNA sequence analysis. (**E**) IKK2 protein is undetectable in IKK2$^{-/-}$ MEF cells. Protein immunoblot analyses of 40 μg of whole-cell extracts from IKK2$^{+/+}$, IKK2$^{+/-}$, and IKK2$^{-/-}$ MEF cells were performed with antibodies to IKK2, IκBα, IκBβ, and IKK1. All antibodies are from Santa Cruz Biotechnology, Santa Cruz, California.

and E14 (Table 1). We conclude that IKK2 is essential during embryonic development at E12.5 to E13.5.

To access if exons Ea and Eb (Fig. 1A) (which encode part of the kinase domain) were deleted, we performed a reverse transcription–polymerase chain reaction (RT-PCR) diagnosis on mouse embryonic fibroblast (MEF) cells isolated from E12.5 IKK2$^{-/-}$ embryos. A pair of primers spanning exons Ea and Eb amplified a 610–base pair (bp) fragment from IKK2$^{+/+}$ cells and a 397-bp fragment from IKK2$^{-/-}$ cells (Fig. 1D). A sequence analysis of the RT-PCR fragments showed that the IKK2 mRNA transcript from IKK2$^{-/-}$ MEF cells contained an in-frame deletion of nucleotides 106 through 318. However, protein immunoblot analysis of the whole-cell extracts with an antibody that recognizes the COOH-terminus of IKK2 failed to detect IKK2 protein. Expression of IKK1, IκBα, and IκBβ was not affected (Fig. 1E). These data indicated that IKK2$^{-/-}$ embryos did not synthesize IKK2 protein.

As a consequence of the loss of IKK2 gene product, mutant mice appeared to suffer severe liver degeneration at the gestation stage. Before E12.5, most IKK2$^{-/-}$ embryos showed no morphological abnormality. At E13 to E13.5, the surviving IKK2$^{-/-}$ embryos showed normal body size and morphology, but their livers appeared smaller and darker (Fig. 2, A and B). The dead or dying IKK2$^{-/-}$ embryos exhibited massive liver hemorrhaging (Fig. 2, C and D) and degeneration (Fig. 2, E and F). Histological examinations revealed that hepatocytes had visible pyknotic nuclei in IKK2$^{-/-}$ embryos, but hematopoiesis appeared normal because many nucleated and enucleated erythrocytes were present. To determine if cell death was apoptotic, we conducted a terminal deoxytransferase-mediated deoxyuridine triphosphate nick-end labeling (TUNEL) assay, and extensive TUNEL-positive cells were identified in IKK2$^{-/-}$ liver cells (Fig. 2, G and H). This result suggested that hepatocyte apoptosis might be a major cause of lethality in the IKK2$^{-/-}$ embryos.

To evaluate whether a loss of IKK2 abolishes signal-induced IκB phosphorylation

Table 1. Genotype of the offspring obtained by the intercross of IKK2$^{+/-}$ mice. Embryos were genotyped by PCR amplification with DNA extracted from the yolk sac and primers c, d, and e (Fig. 1A) (*8*). Detection of heartbeat was used to determine the viability of the embryos. P0, postnatal day 0; dash, data not available.

Stage	Genotype				Total
	+/+	+/−	−/−		
			Alive	Dead	
E12	3	3	1	0	7
E12.5	6	13	10	1	30
E13	9	24	9	5	47
E13.5	7	13	4	4	28
E14	7	6	0	3	16
E14.5	4	5	0	4	13
P0	31	56	0	–	87

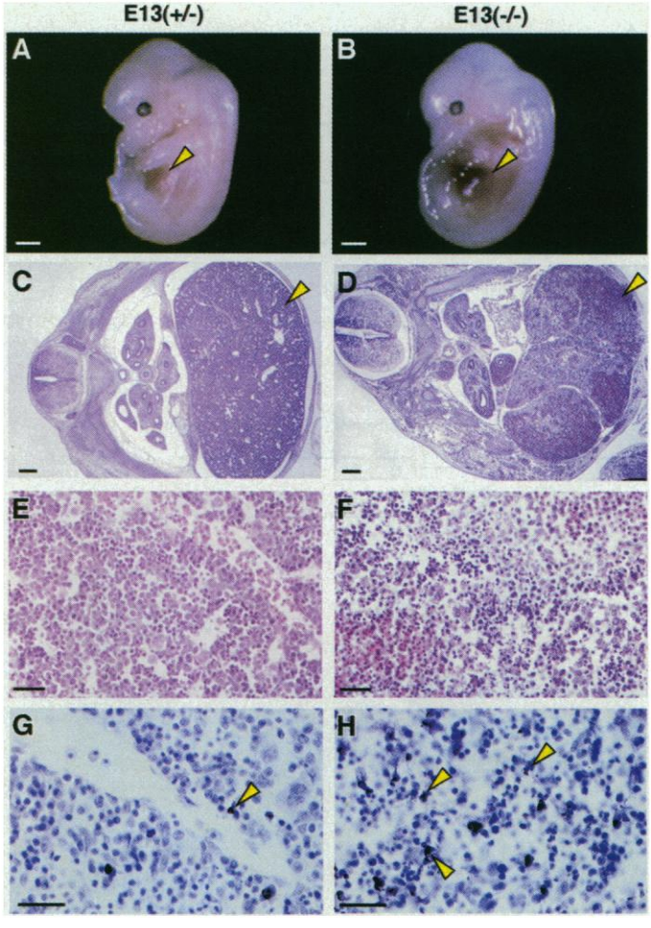

Fig. 2. Liver phenotype in IKK2$^{-/-}$ embryos at E13. For histology, the embryos were fixed in 4% paraformaldehyde at 4°C for 12 hours, dehydrated, and embedded in paraffin. Sections with a thickness of 7 μm were cut and stained with hematoxylin and eosin (HE). (**A**, **C**, **E**, and **G**) Photographs of IKK2$^{+/-}$ embryos at E13. (**B**, **D**, **F**, and **H**) IKK2$^{-/-}$ embryos from the same litter. No differences were detected between IKK2 wild-type and heterozygous embryos. Whole embryos at E13 are shown at low-power magnification in (A) and (B). Many IKK2$^{-/-}$ embryos at this stage showed hemorrhaging in the liver. HE-stained transverse sections of liver are shown in (C) and (D). Hemorrhaging was observed in the liver of IKK2$^{-/-}$ embryos. Arrowheads in (A), (B), (C), and (D) point to the liver. High-power views of the liver in (C) and (D) are shown in (E) and (F), respectively. Hepatocytes in IKK2$^{-/-}$ embryos appear dissociated and dying. Increased cell apoptosis in the liver of IKK2$^{-/-}$ embryos was confirmed by TUNEL assay, as shown in (G) and (H); arrowheads point to the TUNEL-positive apoptotic cells. TUNEL assays were performed on E13 transverse paraffin sections with the ApopTag in situ apoptosis detection kit (Oncor, Gaithersburg, Maryland). Incorporation of digoxigenin-labeled uridine 5′-triphosphate was detected with peroxidase-conjugated sheep anti-digoxigenin Fab fragments (Boehringer Mannheim) (diluted 1:300 in blocking buffer) and visualized by a diaminobenzidine reaction (Boehringer Mannheim). Sections were counterstained with hematoxylin. Scale bars are 1 mm in (A) and (B), 200 μm in (C) and (D), and 70 μm in (E), (F), (G), and (H).

and degradation, inhibiting the activation of NF-κB proteins, we performed a gel shift analysis with nuclear extracts from MEF cells that were untreated or treated with TNF-α and IL-1α. With a human immunodeficiency virus (HIV)–κB–binding site as a probe (*9, 10*), DNA-binding activity was detected in extracts from stimulated IKK2$^{+/+}$ and IKK2$^{+/-}$ MEF cells (Fig. 3A). In contrast, less HIV-κB binding was observed in extracts from stimulated IKK2$^{-/-}$ MEF cells (Fig. 3A). The kinetics of DNA-binding activity mirrored that of the degradation of IκBα and IκBβ (Fig. 3B). Both IκBα and IκBβ were more stable in the extracts of IKK2$^{-/-}$ cells than in those of IKK2$^{+/+}$ and IKK2$^{+/-}$ cells.

Synthesis of IκBα is autoregulated (*5, 11*). After NF-κB activation, one of the first transcribed genes is the gene encoding IκBα. After the addition of TNF-α, newly synthesized IκBα transcripts were detected in IKK2$^{+/+}$ and IKK2$^{+/-}$ MEF cells, whereas only half the amount of induced IκBα mRNA was observed in IKK2$^{-/-}$ MEF cells (Fig. 3C). Generally, the loss of IKK2 did not affect TNF-α–initiated signaling because phosphorylation of c-*Jun*, a member of the AP1 family of transcription factors, was not affected (Fig. 3D). These data showed that TNF-α– and IL-1α–induced activation of NF-κB was impaired in IKK2$^{-/-}$ MEF cells.

Cells lacking NF-κB activity have been shown to undergo apoptosis in response to TNF-α (*10, 12*). Because IKK2$^{-/-}$ mice had impaired NF-κB activity, we investigated whether IKK2$^{-/-}$ MEF cells displayed increased apoptosis upon stimulation with TNF-α. Our data indicated that IKK2$^{-/-}$ MEF cells were much more sensitive to TNF-α–induced apoptosis than cells from wild-type or heterozygous littermates were (Fig. 3E).

Expression of TNF-α has been demonstrated in normal mouse hepatocytes and tumor necrosis factor receptor 1 (TNFR1) is necessary in TNF-α–induced apoptosis in multiple cell types (*13*). To test if the increased hepatocyte apoptosis in IKK2$^{-/-}$ embryos resulted from the TNF-α–induced toxicity, we crossed IKK2$^{+/-}$ mice with TNFR1$^{-/-}$ mice (Jackson Laboratory, Bar Harbor, Maine) to generate IKK2$^{+/-}$/TNFR1$^{+/-}$ double-heterozygous mice that were in turn intercrossed to create the double-mutant mice. Seven of 25 pups born from IKK2$^{+/-}$/TNFR1$^{-/-}$ intercrossing were IKK2$^{-/-}$ mice. Surprisingly, double-mutant embryos developed to term rather than dying around E12.5 to E13.5. However, all the double-mutant neonates died in the first postnatal month. Rescue of embryonic lethality of IKK2 deficiency by inactivation of TNFR1 gene supports our hypothesis that IKK2$^{-/-}$ mice died because of TNF-α–induced hepatocyte apoptosis.

The residual NF-κB activity in response to TNF-α in IKK2$^{-/-}$ cells (Fig. 3A) may have been due to IKK1 or other components of the IKK complex. Recently, NF-κB essential modulator (NEMO) was shown to be a component in the IKK complex and essential for activating NF-κB (*14*). To test if a loss of IKK2 influences the formation of the IKK complex, we immunoprecipitated NEMO complexes from IKK2$^{+/+}$, IKK2$^{+/-}$, and IKK2$^{-/-}$ MEF cell extracts, which were then analyzed by protein immunoblot with antibody to IKK1. IKK1 protein was immunoprecipitated with NEMO in both IKK2$^{+/+}$ and IKK2$^{-/-}$ MEF cells (Fig. 4A). Although in vitro studies suggested that NEMO associates preferentially with IKK2 and not IKK1 (*14*), our data suggest that, in vivo, IKK1 associates with NEMO through a component other than IKK2 in the IKK complex. To determine whether IKK complexes in IKK2$^{-/-}$ MEF cells phosphorylated IκBα upon stimulation with TNF-α or IL-1α, we immunoprecipitated IKK complexes with antibodies to IKK1 (Fig. 4B) or antibodies to NEMO (Fig. 4C) from whole-cell extracts and then we tested them for their ability to phosphorylate IκBα [glutathione S-transferase (GST)–IκBα (amino acids 1 through 54)]. The immunocomplexes from IKK2$^{+/+}$ MEF cells, but not from IKK2$^{-/-}$ MEF cells, phosphorylated GST-IκBα (amino acids 1 through 54) (Fig. 4, B and C). It is possible that an antibody to IKK1 blocks IKK1 kinase activity, so we used an antibody to IKK1 to immunoprecipitate the IKK1 complexes,

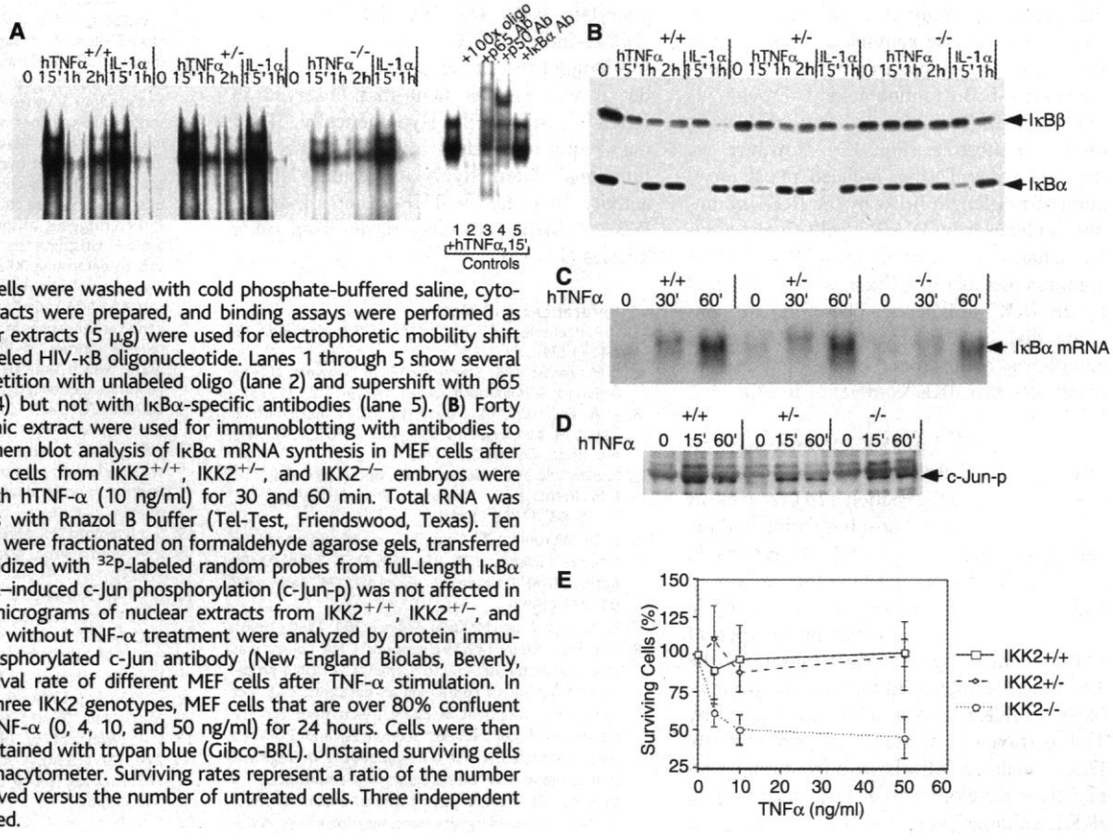

Fig. 3. NF-κB activation by TNF-α and IL-1α in the MEF cells from IKK2$^{+/+}$, IKK2$^{+/-}$, and IKK2$^{-/-}$ mice. (**A**) In 10-cm plates, MEF cells that are over 90% confluent were treated with hTNF-α (10 ng/ml) or human IL-1α (2 ng/ml) for the indicated times (′, min; h, hour). After treatment, cells were washed with cold phosphate-buffered saline, cytoplasmic and nuclear extracts were prepared, and binding assays were performed as described (*9, 10*). Nuclear extracts (5 μg) were used for electrophoretic mobility shift analysis with ^{32}P end-labeled HIV-κB oligonucleotide. Lanes 1 through 5 show several controls, including competition with unlabeled oligo (lane 2) and supershift with p65 (lane 3) and p50 (lane 4) but not with IκBα-specific antibodies (lane 5). (**B**) Forty micrograms of cytoplasmic extract were used for immunoblotting with antibodies to IκBα and IκBβ. (**C**) Northern blot analysis of IκBα mRNA synthesis in MEF cells after TNF-α stimulation. MEF cells from IKK2$^{+/+}$, IKK2$^{+/-}$, and IKK2$^{-/-}$ embryos were untreated or treated with hTNF-α (10 ng/ml) for 30 and 60 min. Total RNA was prepared from MEF cells with Rnazol B buffer (Tel-Test, Friendswood, Texas). Ten micrograms of total RNA were fractionated on formaldehyde agarose gels, transferred to membranes, and hybridized with ^{32}P-labeled random probes from full-length IκBα cDNA (1.5 kb). (**D**) TNF-α–induced c-Jun phosphorylation (c-Jun-p) was not affected in IKK2$^{-/-}$ MEF cells. Ten micrograms of nuclear extracts from IKK2$^{+/+}$, IKK2$^{+/-}$, and IKK2$^{-/-}$ MEF cells with or without TNF-α treatment were analyzed by protein immunoblotting with anti-phosphorylated c-Jun antibody (New England Biolabs, Beverly, Massachusetts). (**E**) Survival rate of different MEF cells after TNF-α stimulation. In six-well plates from all three IKK2 genotypes, MEF cells that are over 80% confluent were stimulated with hTNF-α (0, 4, 10, and 50 ng/ml) for 24 hours. Cells were then treated with trypsin and stained with trypan blue (Gibco-BRL). Unstained surviving cells were counted with a hemacytometer. Surviving rates represent a ratio of the number of treated cells that survived versus the number of untreated cells. Three independent experiments were analyzed.

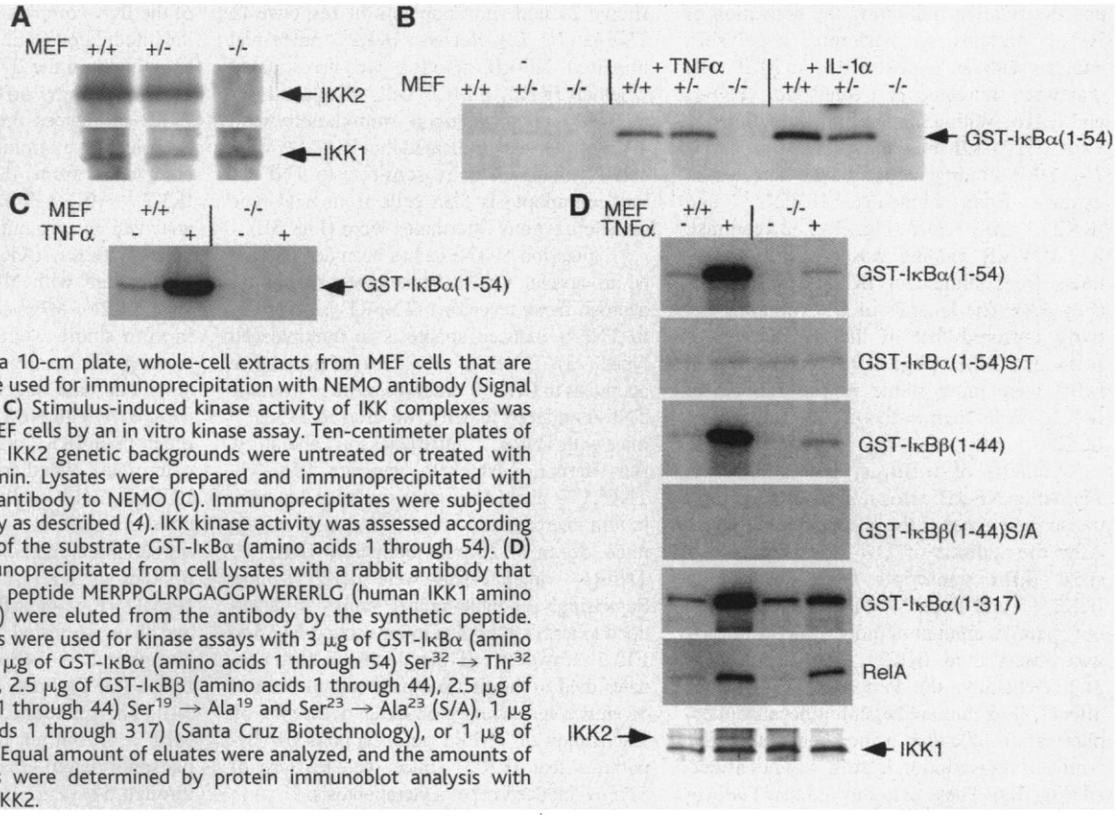

Fig. 4. TNF-α–induced kinase activity of the IKK complex is impaired in the absence of IKK2. (**A**) IKK1 and NEMO are in the same complex in the absence of IKK2. Whole-cell lysates were immunoprecipitated with antibody to NEMO and then immunoblotted with antibodies to IKK1 and IKK2 (Santa Cruz Biotechnology). In a 10-cm plate, whole-cell extracts from MEF cells that are over 95% confluent were used for immunoprecipitation with NEMO antibody (Signal Pharmaceutical). (**B** and **C**) Stimulus-induced kinase activity of IKK complexes was determined in IKK2$^{-/-}$ MEF cells by an in vitro kinase assay. Ten-centimeter plates of MEF cells from different IKK2 genetic backgrounds were untreated or treated with TNF-α or IL-1α for 7 min. Lysates were prepared and immunoprecipitated with antibody to IKK1 (B) or antibody to NEMO (C). Immunoprecipitates were subjected to an in vitro kinase assay as described (*4*). IKK kinase activity was assessed according to the phosphorylation of the substrate GST-IκBα (amino acids 1 through 54). (**D**) Proteins that were immunoprecipitated from cell lysates with a rabbit antibody that recognizes the synthetic peptide MERPPGLRPGAGGPWERERLG (human IKK1 amino acids 1 through 22) (*19*) were eluted from the antibody by the synthetic peptide. Equal amounts of eluates were used for kinase assays with 3 μg of GST-IκBα (amino acids 1 through 54), 1.5 μg of GST-IκBα (amino acids 1 through 54) $Ser^{32} \rightarrow Thr^{32}$ and $Ser^{36} \rightarrow Thr^{36}$ (S/T), 2.5 μg of GST-IκBβ (amino acids 1 through 44), 2.5 μg of GST-IκBβ (amino acids 1 through 44) $Ser^{19} \rightarrow Ala^{19}$ and $Ser^{23} \rightarrow Ala^{23}$ (S/A), 1 μg of GST-IκBα (amino acids 1 through 317) (Santa Cruz Biotechnology), or 1 μg of p65/RelA as a substrate. Equal amount of eluates were analyzed, and the amounts of IKK1 and IKK2 proteins were determined by protein immunoblot analysis with antibodies to IKK1 and IKK2.

which were then eluted from the antibody with an IKK1-specific peptide against which the IKK1 antibody was generated (*15*). Again, little kinase activity was observed in IKK1 immunocomplexes from IKK2$^{-/-}$ cells when GST-IκBα (amino acids 1 through 54) or GST-IκBβ (amino acids 1 through 44) was used as a substrate (Fig. 4D). However, we detected some TNF-α–induced phosphorylation of full-length IκBα by the IKK1 immunocomplexes from IKK2$^{-/-}$ cells. Interestingly, induced phosphorylation of RelA/p65, a common member of NF-κB, was not affected by the IKK2 deficiency. Therefore, we conclude that, in the absence of IKK2, IKK complexes retain some kinase activity but much less than IKK complexes in IKK2$^{+/+}$ MEF cells.

The phenotype of IKK2$^{-/-}$ mice is reminiscent of the RelA/p65$^{-/-}$ mice that die around day 15 of gestation (*16*). A lack of IKK2 might prevent phosphorylation and the subsequent degradation of IκB proteins in response to stimuli, and therefore, a lack of IKK2 prevents the activation of RelA/p65 in liver cells. Rescue of lethal phenotypes of IKK2$^{-/-}$ mice by the inactivation of the TNFR1 gene suggested that hepatocyte apoptosis in IKK2$^{-/-}$ liver cells was induced by TNF-α toxicity, which was prevented by IKK2-mediated NF-κB activity during normal liver development. It is interesting that IKK1, although present in IKK2$^{-/-}$ cells, was unable to substitute for IKK2 function, because both kinases have been shown to phosphorylate IκBα (*7*). We did detect some TNF-α–induced IKK1 kinase activity with full-length IκBα or p65 protein as a substrate, but it was weaker than that observed in IKK2$^{+/+}$ MEF cells. Hypothetically, IKK1 may require activation by IKK2 to be fully functional. Alternatively, the residual NF-κB activity induced by TNF-α and IL-1α in IKK2$^{-/-}$ MEF cells may result from other kinases (*17, 18*).

References and Notes

1. P. A. Baeuerle and T. Henkel, *Annu. Rev. Immunol.* **12**, 141 (1994).
2. I. M. Verma, J. K. Stevenson, E. M. Schwarz, D. Van Antwerp, S. Miyamoto, *Genes Dev.* **9**, 2723 (1995).
3. J. A. Didonato, M. Hayakawa, D. M. Rothwarf, E. Zandi, M. Karin, *Nature* **388**, 548 (1997); C. H. Regnier *et al.*, *Cell* **90**, 373 (1997).
4. F. Mercurio *et al.*, *Science* **278**, 860 (1997).
5. I. M. Verma and J. Stevenson, *Proc. Natl. Acad. Sci. U.S.A.* **94**, 11758 (1997).
6. J. D. Woronicz, X. Gao, Z. Cao, M. Rothe, D. V. Goeddel, *Science* **278**, 866 (1997); E. Zandi, D. M. Rothwarf, M. Delhase, M. Hayakawa, M. Karin, *Cell* **91**, 243 (1997).
7. E. Zandi, Y. Chen, M. Karin, *Science* **281**, 1360 (1998).
8. A mouse strain 129/SVJ genomic DNA library was screened with a full-length human IKK2 cDNA probe. A targeting vector containing an upstream 3-kb Not I to Xho I fragment, a downstream 5-kb Eco RV fragment of homologous sequences, and PGK-neo was constructed. A 3-kb IKK2 genomic DNA fragment that contains two exons coding for amino acids 36 through 106 including Lys^{44}, the adenosine triphosphate (ATP)–binding site necessary for kinase activity, was replaced with the PGK-neo cassette in the sense orientation. Linearized targeting construct was electroporated into J1 ES cells, which were then cultured in G418 (0.2 mg/ml, active form) and 5′-Iodo-2′-fluro-2′ deoxy-1β-D-arabinofuranosyl-5′-Iodouracil (200 μM) media for 8 days. Double-resistant ES cell colonies were selected, and their DNA was analyzed by Southern blot analysis. Six independent targeted ES cell lines with only a single insertion were injected into C57BL/6 strain blastocysts, and heterozygous mutant mice were generated from two of those lines. Mating chimeras with mice of the C57BL/6J strain generated animals with a mixed background. F_1 heterozygous offspring were intercrossed to generate F_2 offspring that were genotyped by PCR analysis to determine IKK2-knockout status. The following primers were used: forward primer c (5′-GGAGAGAAGACAAACATAGTG), which anneals to the genomic sequences in the 5′ arm homologous region; reverse primer d (5′-GTGTCATCCTTGTAGCCATAGT), which anneals to the deleted part of the genomic sequences; and reverse primer e (5′-GGGAACTTCCTGACTAGGGG), which is located within the PGK promoter in the PGK-neo cassette. About 300-bp PCR products were generated from the wild-type allele with primers c and d, whereas an ~250-bp fragment was produced from the targeted allele with primers c and e.
9. S. Miyamoto, M. Maki, M. J. Schmitt, M. Hatanaka, I. M. Verma, *Proc. Natl. Acad. Sci. U.S.A.* **91**, 12740 (1994).
10. D. J. Van Antwerp, S. J. Martin, T. Kafri, D. R. Green, I. M. Verma, *Science* **274**, 787 (1996).
11. S.-C. Sun, P. A. Ganchi, D. W. Ballard, W. C. Greene, *ibid.* **259**, 1912 (1993); M. L. Scott, T. Fujita, H. C. Liou, G. P. Nolan, D. Baltimore, *Genes Dev.* **7**, 1266 (1993); P. J. Chiao, S. Miyamoto, I. M. Verma, *Proc. Natl. Acad. Sci. U.S.A.* **91**, 28 (1994).
12. C.-Y. Wang, M. W. Mayo, A. S. Baldwin Jr., *Science* **274**, 784 (1996); A. A. Beg and D. Baltimore, *ibid.*, p. 782; Z. G. Liu, H. Hsu, D. V. Goeddel, M. Karin, *Cell* **87**, 565 (1996);
13. J. S. Hunt, H. L. Chen, X. L. Hu, T. Y. Chen, D. C.

Morrison, *Cytokine* **4**, 340 (1992); M. Tewari and V. M. Dixit, *Curr. Opin. Genet. Dev.* **6**, 39 (1996).
14. S. Yamaoka *et al.*, *Cell* **93**, 1231 (1998); D. M. Rothwarf, E. Zandi, G. Natoli, M. Karin, *Nature* **395**, 297 (1998); F. Mercurio *et al.*, *Mol. Cell. Biol.* **19**, 1526 (1999).
15. Three 15-cm plates of MEF cells from IKK2$^{+/+}$ and IKK2$^{-/-}$ mice were untreated or treated with human TNF-α (hTNF-α) (10 ng/ml) for 7 min. Whole-cell lysates from each 15-cm plate were prepared and immunoprecipitated with 10 μl of antibody to IKK1 in 1 ml of immunoprecipitation (IP) buffer (*4*). Twenty microliters of protein A were added and samples were rotated for 2 hours at 4°C. The immunoprecipitates were then washed three times with IP buffer. Samples from all three 15-cm plates were pooled into one tube and washed once with kinase assay (KA) buffer (*4*). Sixty micrograms of synthetic peptide in 140 μl of KA buffer were added to the protein A beads and samples were rotated for 6 hours at 4°C. After a brief spin, the eluates were transferred to new tubes. Twenty microliters of eluates were used for each KA reaction or protein immunoblot analysis.
16. A. A. Beg, W. C. Sha, R. T. Bronson, S. Ghosh, D. Baltimore *Nature* **376**, 167 (1995).
17. M. Hirano *et al.*, *J. Biol. Chem.* **271**, 13234 (1996).
18. V. Imbert *et al.*, *Cell* **86**, 787 (1996).
19. Single-letter abbreviations for the amino acid residues are as follows: A, Ala; E, Glu; G, Gly; L, Leu; M, Met; P, Pro; R, Arg; and W, Trp.
20. We thank Y. Marchuk and B. Dominguez for their excellent technical assistance, A. Israel for NEMO antibody, and B. Coyne for her help with this manuscript. We also thank the following people for their expertise, discussions, and sustained interest in our work: Q. Lu, S. Crone, J. C. Izpisúa Belmonte, members of the Verma laboratory, and M. Hoekstra, D. Anderson, and A. Lewis of Signal Pharmaceuticals. Q.L. is supported by a training grant from NIH, K.-F.L. is a Pew Scholar and is supported by NIH and the March of Dimes Foundation, and I.M.V. is an American Cancer Society Professor of Molecular Biology and is supported by the Valley Foundation and grants from NIH.

15 December 1998; accepted 12 March 1999

Evolution of a Protein Fold in Vitro

Matthew H. J. Cordes,[1] Nathan P. Walsh,[1] C. James McKnight,[2] Robert T. Sauer[1]*

A "switch" mutant of the Arc repressor homodimer was constructed by interchanging the sequence positions of a hydrophobic core residue, leucine 12, and an adjacent surface polar residue, asparagine 11, in each strand of an intersubunit β sheet. The mutant protein adopts a fold in which each β strand is replaced by a right-handed helix and side chains in this region undergo significant repacking. The observed structural changes allow the protein to maintain solvent exposure of polar side chains and optimal burial of hydrophobic side chains. These results suggest that new protein folds can evolve from existing folds without drastic or large-scale mutagenesis.

Protein sequences in biological systems evolve by random mutation, including substitutions and en bloc changes resulting from frameshifts or large insertions and deletions. Such genetic changes can result, at least occasionally, in structural evolution to a new or dramatically different three-dimensional (3D) fold (*1*). Little is known, however, about how many or what kind of sequence changes might lead to significant structural changes. Mutagenesis experiments show that limited changes in sequence can have large effects on stability and activity, but generally do not lead to large shifts in structure. For example, highly disruptive mutations such as insertions in elements of regular secondary structure or hydrophobic-to-charged substitutions at core positions lead to only minor structural differences in bacteriophage T4 lysozyme and staphylococcal nuclease, pointing to a strong drive to preserve the basic native fold (*2*, *3*). Here, by contrast, we show that mutations at adjacent positions in the antiparallel β sheet of Arc repressor are sufficient to change the local secondary structure to a right-handed helix without loss of global protein stability or folding cooperativity. This suggests that it is plausible to evolve a new protein fold from an existing fold by the accumulation of simple substitution mutations.

The wild-type Arc repressor homodimer (*4*) contains an antiparallel β sheet consisting of a single strand of sequence Gln^{9}-Phe^{10}-Asn^{11}-Leu^{12}-Arg^{13}-Trp^{14} from each monomer. The odd-numbered side chains are polar, solvent-exposed, and form the surface of Arc that binds operator DNA. The even-numbered side chains are hydrophobic, buried in the protein core, and are crucial for Arc folding and stability (*5*). By interchanging Asn^{11} and Leu^{12}, a surface residue and an adjacent core residue, respectively, we constructed "switch" Arc, a mutant with the same amino acid composition as the wild type but with a different binary pattern of polar and hydrophobic side chains in the β-sheet region.

The purified wild-type and switch Arc proteins differ in their far-ultraviolet circular dichroism (CD) spectra (Fig. 1A), near-ultraviolet CD spectra (Fig. 1B), and fluorescence spectra (Fig. 1C), suggesting that the switch mutations alter the normal Arc fold (*6*). In

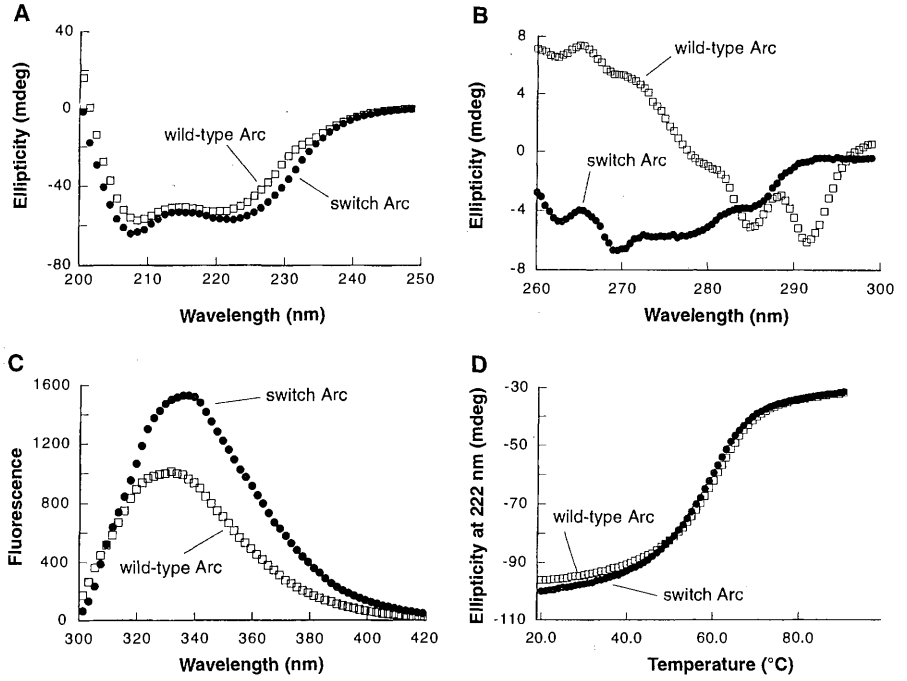

Fig. 1. Biophysical properties of wild-type and switch Arc. (**A**) Far-ultraviolet CD spectra (50 μM protein, 15°C), (**B**) near-ultraviolet CD spectra (100 μM protein, 15°C), (**C**) tryptophan fluorescence emission spectra (50 μM protein, 25°C), and (**D**) CD thermal denaturation curves (10 μM protein). The CD signal is expressed in millidegrees of rotation.

[1]Department of Biology, Massachusetts Institute of Technology, Cambridge, MA 02139, USA. [2]Department of Biophysics, Boston University School of Medicine, Boston, MA 02118, USA.

*To whom correspondence should be addressed. E-mail: bobsauer@mit.edu